Micromachined Deformable Mirrors for Dynamic Wavefront Control

Thomas Bifano[a] , Paul Bierden[b] Julie Perreault[c] and
[a]Manufacturing Engineering, Boston University, MA 02215
[b]Boston Micromachines Corporation, Watertown, MA 02472
[c] Electrical and Computer Engineering, Boston University, MA 02215

1. Abstract

The design, manufacture, and testing of optical quality surface micromachined deformable mirrors (DMs) is described. With such mirrors, the shape of the reflective surface can be modified dynamically to compensate for optical aberrations and thereby improve image resolution in telescopes or microscopes. Over several years, we have developed microelectromechanical system (MEMS) processing technologies that allow production of optical quality of surface micromachined mirrors. These process steps have been integrated with a commercial foundry process to produce deformable mirrors of unprecedented quality. The devices employ 140 electrostatic actuators. Measurements of their performance detailed in this paper include 2μm of useful stroke, 3nm position repeatability, >90% reflectivity, and flatness better than 20nm RMS. A chemo-mechanical polishing process has been used to improve surface quality of the mirrors, and a gold coating process has been developed to improve the reflectivity without introducing a significant amount of stress in the mirror membrane. An ion bombardment technique has been developed to flatten mirrors. These silicon based deformable mirrors have the potential to modulate spatial and temporal features of an optical wavefront, and have applications in imaging, beam-forming, and optical communication systems. Design considerations and performance evaluation of recently fabricated DMs are presented.

Keywords – Adaptive optics, deformable mirror, MOEMS
Corresponding Author: Thomas Bifano, Professor and Chair, Manufacturing Engineering Department, Boston University, 15 Saint Mary's Street, Brookline, MA 02446,
Telephone: (617)-529-1533, Fax: (617) 353-5548, Email: tgb@bu.edu

2. Introduction

In an AO system, a wavefront corrector intercepts the propagating wavefront in a plane conjugate to the optical pupil. The wavefront corrector modifies the spatial phase of the wavefront, compensating for some or all of it's accumulated, undesired phase aberrations. The most common type of wavefront corrector used in AO is a deformable mirror (DM), which adjusts phase using an array of spatially distributed actuators that deform a continuous or segmented reflective surface. Each actuator in the DM provides a degree of freedom in altering contour shape or phase of the propagating wavefront. The typical goal in AO control is to alter the DM's shape so that the reflected wavefront from a distant point source is made planar, thereby compensating aberrations in the optical beam path. Important electromechanical characteristics of the DM – including number of actuators, actuator stroke, actuator resolution, and actuation speed – are determined by the character of the aberrations that need to be compensated [1]. For AO in astronomical imaging applications, most DMs

Advanced Wavefront Control: Methods, Devices, and Applications II, edited by John D. Gonglewski, Mark T. Gruneisen, Michael K. Giles, Proceedings of SPIE Vol. 5553 (SPIE, Bellingham, WA, 2004)
0277-786X/04/$15 · doi: 10.1117/12.556690

used to date employ tens to hundreds of actuators, with several microns of maximum stroke, and closed-loop speeds of tens to hundreds of hertz.

Until recently, most DMs were discretely assembled, macroscale systems comprised of a thick flat mirror affixed to an array of spatially-distributed discrete piezoelectric actuators supported on a rigid backplane. For all but a small number of applications, these DMs are prohibitively expensive [2]. Micromachining offers a promising alternative approach for DM manufacture. Potentially, micromachining could decrease the cost of DMs substantially while yielding a device with improved speed and compactness. Moreover, microelectromechanical systems technology could eliminate some of the most significant challenges associated with macroscale DMs: replacing piezoelectric actuators with lower-power electrostatic actuators and replacing a complex assembly process with batch micromachining processes. Potential advantages in performance and cost have launched a number of recent research efforts directed toward producing optical-quality micromachined deformable mirrors (μDMs). While there are advantages and limitations associated with all of the μDMs that have been reported [3], the commercial availability of μDMs is already transforming the field of adaptive optics in areas that can benefit from their high speed, low cost, and compact size. Areas in which μDMs have recently proven successful include astronomy [4], ophthalmic imaging [5,6], vision correction [7-9], laser communication [10-12], microscopy [13] and laser beam enhancement [14,15].

In this paper, an optical-quality silicon micromachined deformable mirror (μDM) and the manufacturing process used to produce it are described, and its performance is evaluated.

Architecture

The device was fabricated using surface micromachining processes on a silicon substrate coated with a thin silicon nitride film for electrical isolation. The structural elements of the μDM (actuators and mirrors) are all polycrystalline silicon (polysilicon). An array of independently addressable, electrostatic actuators provides the driving forces needed to deform the mirror. Each actuator consists of a 300 x300 x 2 μm polysilicon plate anchored to the silicon nitride layer along two of its sides. Each actuator plate is suspended 5μm above a polysilicon electrode patterned onto the silicon nitride layer. Polysilicon routing lines lead from each electrode to the periphery of the chip. Actuation is achieved through electrostatic attraction between the compliant actuator plate, which is electrically grounded, and the rigid electrode beneath it, which has its voltage potential controlled by an external driver. Attached to the center of the top surface of each actuator plate is a 20 x 20 x 2.5 μm post. A mirror plate is attached to the top of this array of posts. A microscope photograph of the 1 cm chip is depicted in Figure 1. Three types of mirror plates have been fabricated, all using the actuator arrays described above. There are *continuous mirrors*, *stress-relieved mirrors*, and *segmented mirrors*.

Continuous mirror devices employ a single polysilicon thin film that spans the entire actuator array in an uninterrupted structure, except for a number of small holes needed for etching the underlying sacrificial layers. When actuated, the mirror assumes a smooth shape without edge discontinuities or abrupt changes in slope – a characteristic that is generally desirable in a DM. Continuous mirror μDMs are susceptible to undesirable deformation due to biaxial stresses (generally compressive) in

the polysilicon induced during fabrication. Stress-relieved mirror devices reduce this effect through the addition of regularly-spaced narrow cuts in the mirror plate between attachment posts, which allows the mirror to expand locally to relieve some biaxial stress. This improves overall mirror flatness but reduces the mirror's fill factor and increases unwanted diffraction. Segmented mirror devices employ a small mirror plate above each actuator, centered on the post. These mirror segments are mechanically decoupled from one another: each moves in a surface-normal direction without influencing its neighbors. Almost all biaxial stresses in the mirror are relieved by this segmentation. Segmented mirror devices have optical characteristics that are suitable for use as micro spatial light modulators, or μSLMS. However, the phase discontinuity that occurs at segment edges when the array is actuated makes them less useful for phase conjugation than the other two types of mirrors, for a given actuator array size.

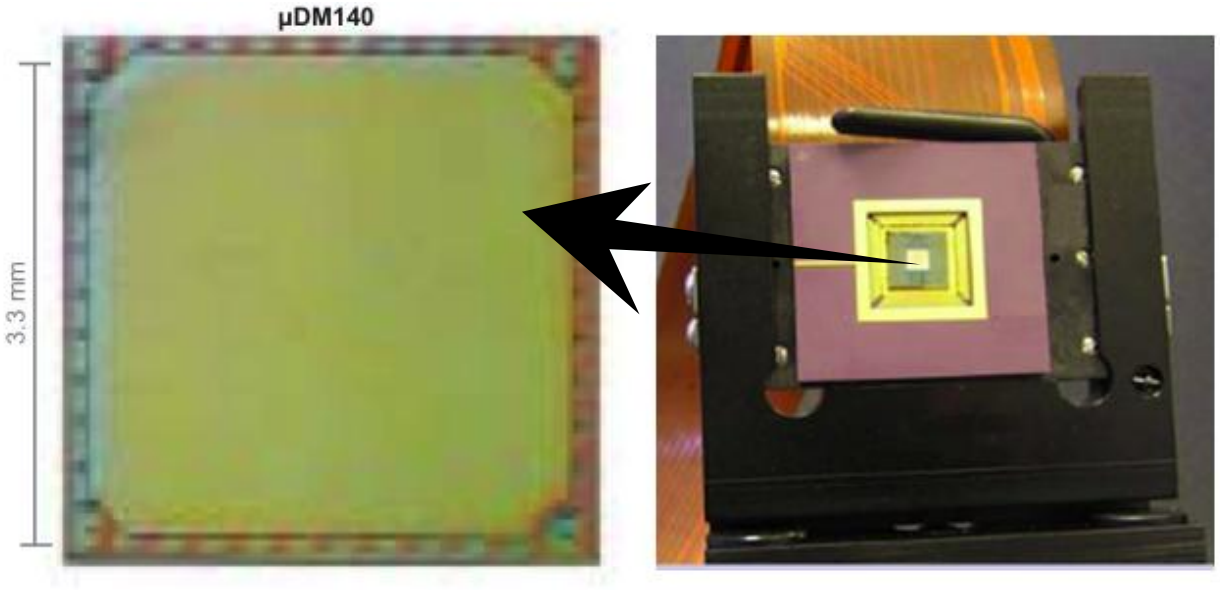

Figure 1. Photographs of packaged deformable mirror device. Left: Image of gold-coated silicon DM. Right: DM in ceramic package, mounted in a zero-insertion force socket on an optical gimbal structure, and connected to the driver (not shown) via a high-density flexible cable.

3. Micromirror Fabrication

The μDM development process spanned several years, during which three generations of micromirrors were developed. Each of these was fabricated in a custom surface micromachining fabrication run. In custom-run I, a parametric study of actuator array geometry was conducted. As a result, an acceptable electrostatic actuator geometry was chosen from hundreds of alternatives. In custom-run II, arrays of these actuators were used as the foundation for dozens of mirror device geometries and architectures. Principle objectives were to reduce print-through and to achieve working arrays of up to 100 elements. Again, the results were used to converge on an acceptable design. Custom-run III produced large numbers of identical working μDMs, and explored fabrication-based approaches to improving mirror optical quality. The custom fabrication processes all used three structural layers of polysilicon (poly) alternating with two sacrificial layers of phosphosilicate glass

(PSG). Table I describes the major steps of the process flow used to make the μDM devices in custom run III. Steps 1 through 9 were performed at a silicon micromachining foundry[1]. The latter two process steps were performed at Boston University.

Table I: Outline of Processing Steps Used

Step	*Process Step*	*Thickness*	*Description*	*Purpose*
1	Nitride	1.0μm	Deposit, pattern, and etch nitride	Electrical insulator
2	Poly 0	0.5μm	Deposit, pattern, and etch polysilicon	Electrode/wire routing
3	Oxide 1	5.0μm	Deposit, pattern, and etch oxide	Sacrificial
4	Poly 1	2.0μm	Deposit, pattern, and etch polysilicon	Actuator plate and anchor
5	Oxide 2	2.5μm	Deposit, pattern, and etch oxide	Sacrificial
6	Chemopolish	-0.2μm	Polish oxide before final poly	Improve surface finish
7	Poly 2	3.0μm	Deposit, pattern, and etch polysilicon	Mirror and posts
8	Pad Metal	0.5μm	Deposit gold on wirebond pads[2]	Wirebond pads
9	Release		Dice and release in HF	Remove sacrificial material
10	Ion Machine		Ion machine poly2 surface	Improve surface flatness
11	Metal	500-1500Å	Evaporate gold on mirror surface	Improve reflectivity

A four inch silicon wafer was used as the substrate. A low stress silicon nitride layer was deposited, lithographically patterned, and etched to allow electrical access to the substrate. The first layer of polysilicon, *poly0,* was deposited, patterned, and etched to create actuator base electrodes and wire routing for the array. A sacrificial layer, *oxide 1,* was deposited, patterned, and etched. This unusually thick layer was used to create the actuator gap and actuator anchors. Another layer of polysilicon, *poly1*, was deposited, patterned, and etched to create anchors and compliant electrode actuator plates. A sacrificial layer, *oxide2*, was deposited, patterned, and etched to serve as a spacer between the actuator and the mirror. A final polysilicon layer, *poly2,* was deposited, patterned, and etched to create the mirror and it's post attachments to the *poly1* actuator. Pad metal was patterned and deposited through a liftoff process to facilitate wire bonding of the device. The wafer was then diced into 10mm square chips. Sacrificial material was removed with an HF etch, releasing the structural polysilicon. The *poly2* surface on each chip was then measured optically for nonplanarity, and ion machined to flatten the mirror. Finally, a reflective coating of gold was vapor-deposited directly on *poly2* though a shadow-mask. Figure 2 is a cross-sectional schematic (one actuator wide) depicting the fabrication process used to create the device.

[1] Although all three custom fabrication runs were performed on essentially the same equipment, the ownership of the foundry service was MCNC, then Cronos, and then JDS Uniphase MEMS Business Unit for the three custom runs, respectively. The foundry is now run by MEMSCAP.
[2] Not depicted in Figure 2

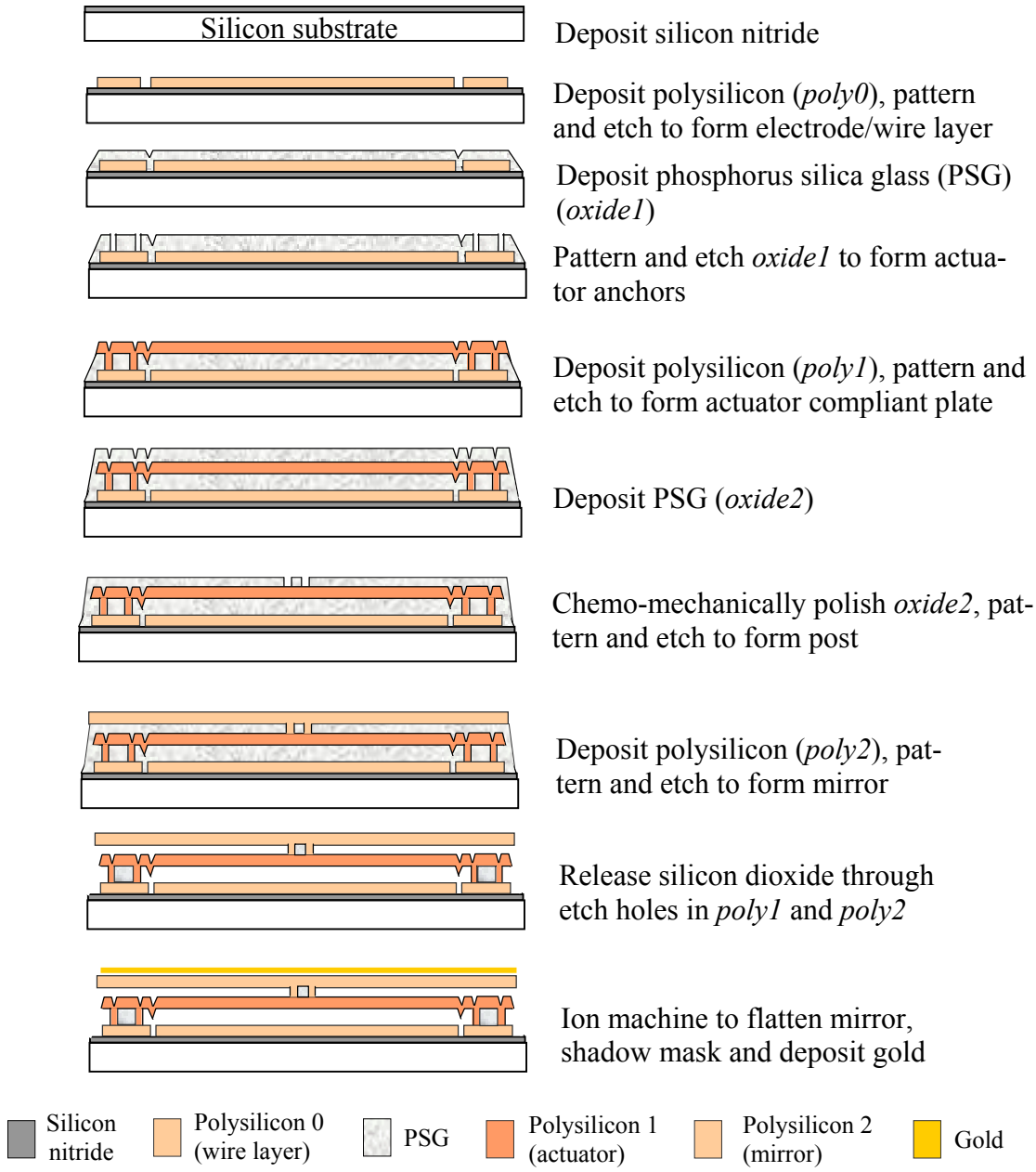

Extensions and modifications to traditional surface micromachining processes were developed to produce optical quality mirrors. These include design-based planarization [17], post-release stress modification by ion machining [18] and low-stress gold coating.

Figure 2: Micromachining processes for the fabrication of a deformable mirror

Design Based Planarization

Design based planarization is a layout strategy used to reduce the buildup of unintended topography in micromachining. Unintended topography is well-known problem in surface micromachining, through which devices are fabricated by sequential deposition and patterning of multiple conformal thin films. Films deposited later in the process are not flat. Their topography is determined by the patterns, holes, and features present in underlying films. Wide cuts in one layer will result in trenches in the subsequent layers, for example. In some micromachined structures, such "print through" has been exploited as a feature, allowing the fabrication of locking hinge pins, for example. For the μDM, it is essential that the final deposited layer is flat enough to serve as an optical quality mirror. Very little print-through from underlying actuator and electrode and post structures can be tolerated.

In design-based planarization, a layout rule limits the buildup of topography by restricting layout patterns so that the width of etched lines never exceeds the *minimum* allowable etch width for the production process (2μm in the micromachining processes used for μDM fabrication). Polysilicon and PSG are highly conformal, hence subsequent layers tend to fill in these narrow cuts and smooth over them. This approach has been used successfully to reducing print-through topography to sub-micrometer levels even after depositing and patterning the four thin films that precede the mirror. To further improve the mirror's optical quality, a chemomechanical polishing process is used to smooth over any remaining print-through in the sacrificial PSG layer upon which the mirror is to be deposited. A more detailed study of the principles behind design-based planarization has been reported previously [17].

Chemo-mechanical Polishing

An important figure of merit for a μDM is the optical quality of the reflecting surface. One common measurement of optical quality is surface RMS roughness. As a rule of thumb, a surface roughness of less than 10nm RMS is required for good optical performance. In surface micromachining techniques, unpolished thin films of polycrystalline silicon typically exhibit surface roughness of ~ 20nm RMS, exclusive of print-through effects. Print-through adds to this roughness. After design based planarization and the fabrication processes described previously (with the exception of chemomechanical polishing) the mirror surface roughness was measured using an atomic force microscope (AFM) at about ~50nm RMS, too rough for use in a typical AO system. A forty second chemomechanical polishing process reduced the surface roughness to approximately 10nm RMS.

Post-release Stress Modification by Ion Bombardment

Design based planarization and chemo-mechanical polishing will result in smooth planar structures pre-release. However, upon release of the structure residual stresses in the structural thin films (particularly residual stress *gradients* through the film's thickness) are partially relieved, resulting in out-of-plane strain (e.g. mirror nonflatness). For the μDMs, a primary cause of the out-of-plane bending is a stress gradient through the thickness of the mirror film. The local curvature of the film can be calculated using a classical mechanics approach in which curvature is related to the internal

cross-sectional moment in the film – a parameter that can be varied by adding removing, or transforming a uniformly biaxially stressed layer (of appropriate magnitude and thickness) of the mirror film. Free-standing released test structures on the wafers were, as processed, slightly cup shaped. It was determined that adding a thin compressive layer at the upper surface of the mirror could be used to flatten the mirror. A broad, uniform argon ion beam was used to bombard the polysilicon mirror film, transforming the structure of its upper 5-10 nanometers from polycrystalline to a less-dense disordered state, and inducing a compressive stress. It was found that such a process could produce predictable, permanent changes in the film sufficient to flatten it. An analytical model of this process and an empirical study of ion-induced stress modification has been reported previously [18]. This approach led to a significant improvement in mirror flatness on μDM devices.

Metallization

Bare silicon has a low reflectivity at visible wavelengths, and is almost transparent at near-infrared wavelengths. As a result, a silicon-based μDM typically needs a reflective coating. Coating the mirror membrane with a highly reflective metallic material can improve reflectivity, but care must be taken not to introduce unacceptable stresses on the mirror surface. Gold was chosen as a coating material because it has a high reflectivity over a relatively wide bandwidth, a relatively low intrinsic stress, and it will not oxidize.

Metalization processes used in polysilicon micromachining foundries have been developed primarily for electrical interconnection. For that purpose, strong surface adhesion is an important attribute of the coating (e.g. to prevent wire-bond delamination). To improve adhesion, gold is usually deposited not on bare silicon but instead on a thin adhesion layer such as chromium. Unfortunately, the same thin film materials that enhance adhesion are almost always highly stressed. As a result, they cause unacceptable deformation of the mirror film. Fortunately, the adhesion required for an optical coating is not comparable to the adhesion required for a wire-bond. Durability of the evaporated gold on piece silicon was evaluated under different temperature conditions. Silicon partially coated in evaporated gold was subjected to ten minute excursions to a maximum anneal temperature of 350°C. After each thermal cycle the reflectivity of the bare silicon and the gold on silicon was evaluated against a front surface mirror. No significant change in the reflectivity of the gold coating was measured. The same piece was then evaluated for a 72 hour anneal at a temperature of 350°C without a significant change in the reflectivity. It was found that gold could be deposited directly on the mirror though a shadow-mask evaporation process *after release* to achieve a highly reflective mirror surface [16]. A highly reflective mirror surface was produced on a continuous mirror membrane with e-beam evaporation without a significant change in the surface roughness or the mirror flatness. Approximately 80 nm of gold was deposited on the mirror surface at a rate of 0.2nm/sec. An optical multimeter was used to measure the reflectivity of the continuous mirror membrane before and after the gold coating. At a wavelength of 632.8nm and an incident optical power of about 8mW. The reflectivity increased from 41% without coating, to 91% with the coating. There was no change in surface roughness after the evaporaton in gold.

4. µDM Device Characterization

After micromachining, stress modification by ion bombardment, and gold coating, a number of µDM devices were bonded by epoxy to ceramic chip carriers and then wirebonded. The devices had nominal geometric properties as defined in Table II:

Table II: Geometry of the Deformable Mirror

Number of actuators	140 (12 x 12 array w/o corners)
Actuator pitch	300µm (fixed-fixed beams)
Mirror geometry	3.3mm square x 3µm thick
Die size	10mm square

The fill factor is 98.6% for the stress-relieved mirrors and segmented mirrors and above 99.5% for the continuous mirrors.

Electromechanical performance of individual actuators was measured in a number of ways. First, actuators were driven quasi-statically, while mirror deflection directly above the actuator center post was measured relative to undeflected regions of the mirror, using a Wyko NT2000 surface mapping interferometric microscope. Voltage-deflection curves for several different actuator locations in the array were measured. The deflection was found to increase monotonically with applied voltage. Reproducible differences in voltage vs. deflection behavior among the different actuators were observed. For example, as seen in Figure 3, when subjected to an actuation voltage of 190V, the most compliant actuator deflected by 2.0µm while the stiffest actuator deflected by 1.9µm, a difference of 100nm. Such differences in behavior from actuator to actuator in the array were found to be consistent with predictions based on measured geometric differences in actuator thickness and actuator gap across the device. In turn, these geometric differences were consistent with the known tolerance limits of the foundry process used in their fabrication

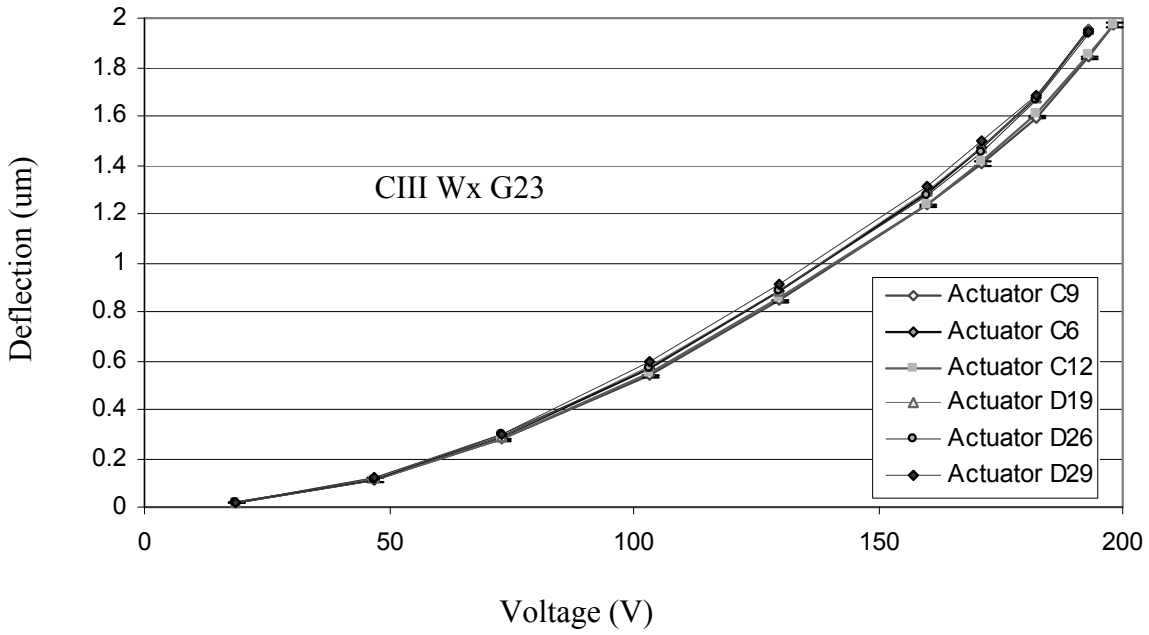

Figure 3: Voltage deflection curves f of a continuous mirror coated with gold

With different actuator geometries based on this same architecture, arrays with as much as 4.0μm of stroke at each actuator have been produced.

Figure 4 illustrates a gray-scale contour map of the deformed portion of the continuous mirror surface while one actuator was energized along with a sectional profile through the contour. It can be seen that the deformation is localized around the energized actuator and extends several hundred micrometers radially. The *influence function* for this actuator, defined as the deflection above an adjacent unenergized actuator as a percentage of the deflection above the energized actuator, is about 15%. The locations of two adjacent actuators are marked by black triangles in Figure 4.

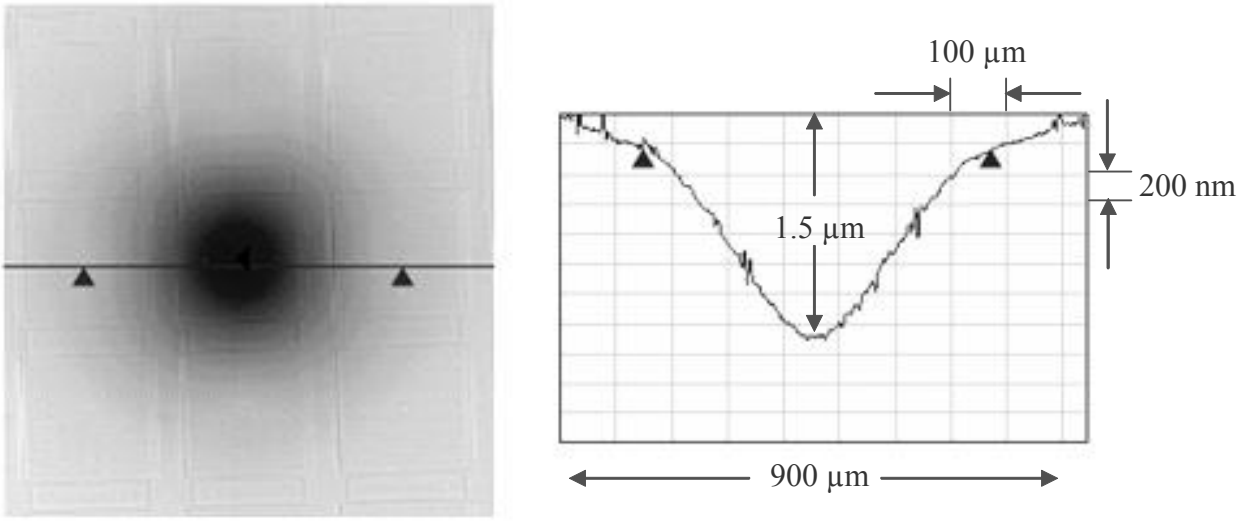

Figure 4: Top surface and cross section of a deflected central actuator.

Position repeatability was measured for a single actuator on the CIII Wx G23 continuous membrane mirror through ensemble averaging of the data from a series of step input tests. Deflections were measured using a Zygo ZMI 1000 single-point displacement dynamic interferometer. This device uses a focused laser beam to measure normal displacement with a position resolution of 2.5nm over a frequency bandwidth of 0-133kHz, and a lateral averaging area of ~30μm.

Ten sets of five sequential measurements taken over several hours at a partial pressure of 200Torr. There were 50 measurements for each data point, for a total of 450 data points per run and 4500 points over the whole experiment. The results, shown in Figure 5, show excellent actuation repeatability. The standard deviation in displacement for each measurement point in the graph is 3nm, close to the measurement resolution of the instrument. This represents a dynamic range of nearly 10^3 for the actuators.

The temporal bandwidth of a continuous membrane deformable mirror was measured in air using the same dynamic interferometer, and driving a single actuator with a 10V sinusoidal input superimposed on a 100V DC offset. The system was modeled and an undamped mechanical resonant frequency of approximately 60kHz was predicted. Air damping significantly reduces the bandwidth of the mirror system, as shown in Figure 6.

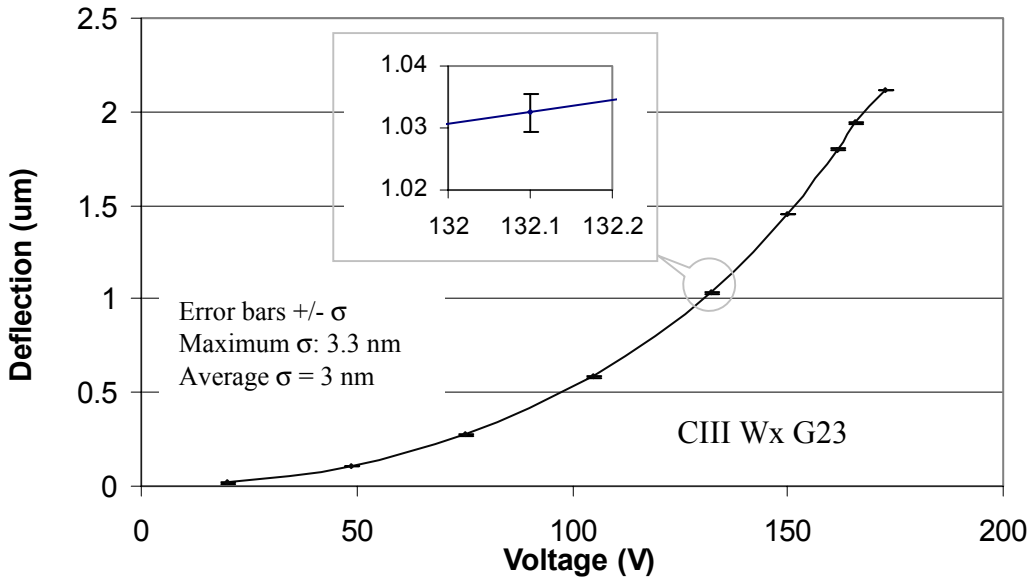

Figure 5: Voltage-deflection repeatability measurements of a single actuator on a continuous mirror

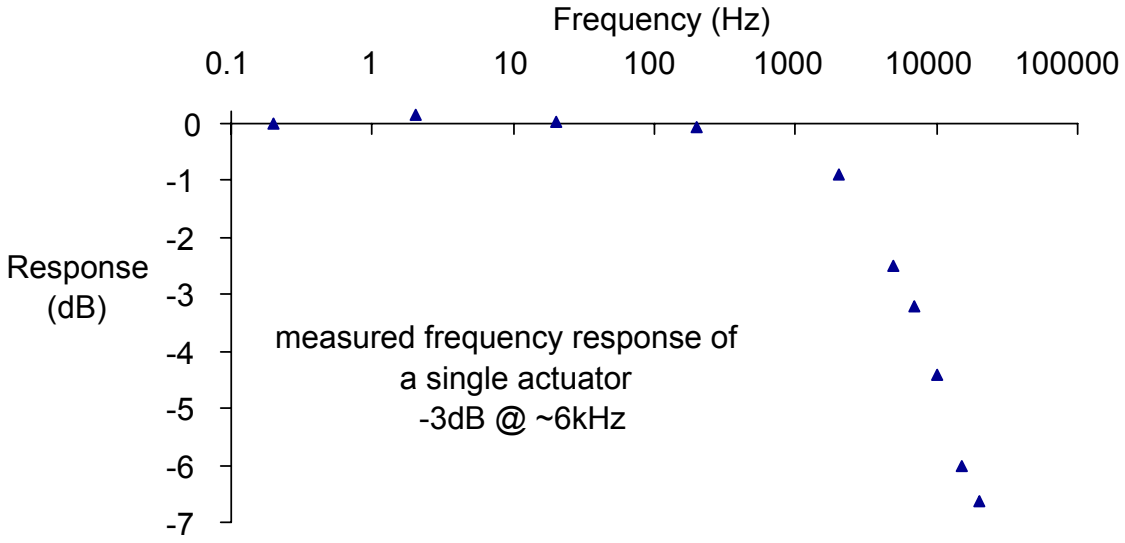

Figure 6: Amplitude response for a continuous mirror membrane

To better understand the effects of air damping on resonant frequency, a vacuum chamber with a viewing window was constructed and used to enclose the mirror system in a partial vacuum environment. A laser vibrometer was used to measure the effect of pressure on the mirror response. An

individual mirror segment was driven with a sinusoidal 1VAC superimposed on a 100VDC offset. In low frequency (~1Hz) measurements in air (for which air damping would not affect motion), this input would cause 25nm of periodic motion. Velocity measurements were taken over a range of input frequencies and integrated to yield displacement data. This experiment was repeated for several different chamber pressures as shown in Figure 7. At atmospheric pressure, the amplitude roll off frequency occurs well below the first resonant frequency. As the pressure is reduced the mirror exhibits an underdamped resonance at ~60kHz.

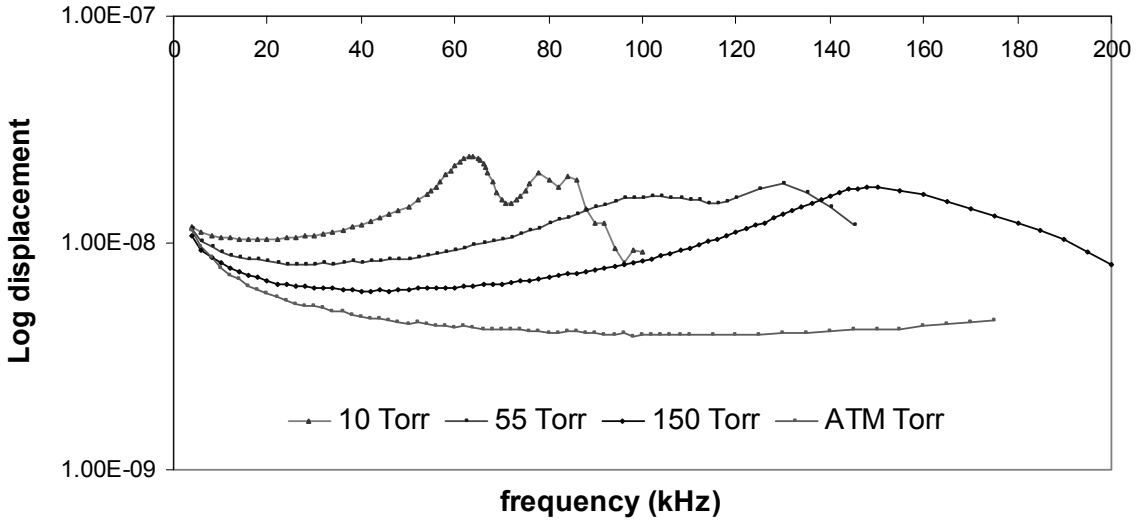

Figure 7: Amplitude response of a sinusoidal input over a range of frequencies for several chamber pressures

5. Demonstration of wavefront control

The μDM 140 device was integrated with a wavefront sensor and a control computer to demonstrate its capacity for controlling an optical wavefront. In this test bed, a helium neon laser was focused on a diffuse target. Light scattered from the target was collected by a lens, and relayed to a μDM in the pupil plane. A telecentric pair of lenses was used to relay the wavefront to a Shack Hartmann sensor located at a conjugate pupil. In this configuration, the mirror surface deforms the incident (planar) wavefront, and the sensor detects local changes in wavefront slope. These slope measurements can be used to estimate the wavefront shape. The amplitude of wavefront deformation is twice the amplitude of the mirror's physical deformation.

Wavefront aberrations are frequently represented mathematically by Zernike polynomials, an orthonormal set of functions defined on a unit circle that are mapped to the pupil of the optical system. Any wavefront aberration can be decomposed into a unique set of coefficients for these Zernike polynomials. Many of the lower-order Zernike polynomials define familiar optical aberrations (tilt, focus, astigmatism, coma, etc.). It is useful to evaluate a wavefront correction device in terms of its capacity to impose individual Zernike polynomial shapes on the wavefront. Using closed-loop control, the deformable mirror was commanded to take on the shape of each of the first

twenty-one polynomial shapes (excluding the first three terms, which represent simple planar translations and rotations of the wavefront). Figure 8 illustrates the measured wavefront produced in these experiments.

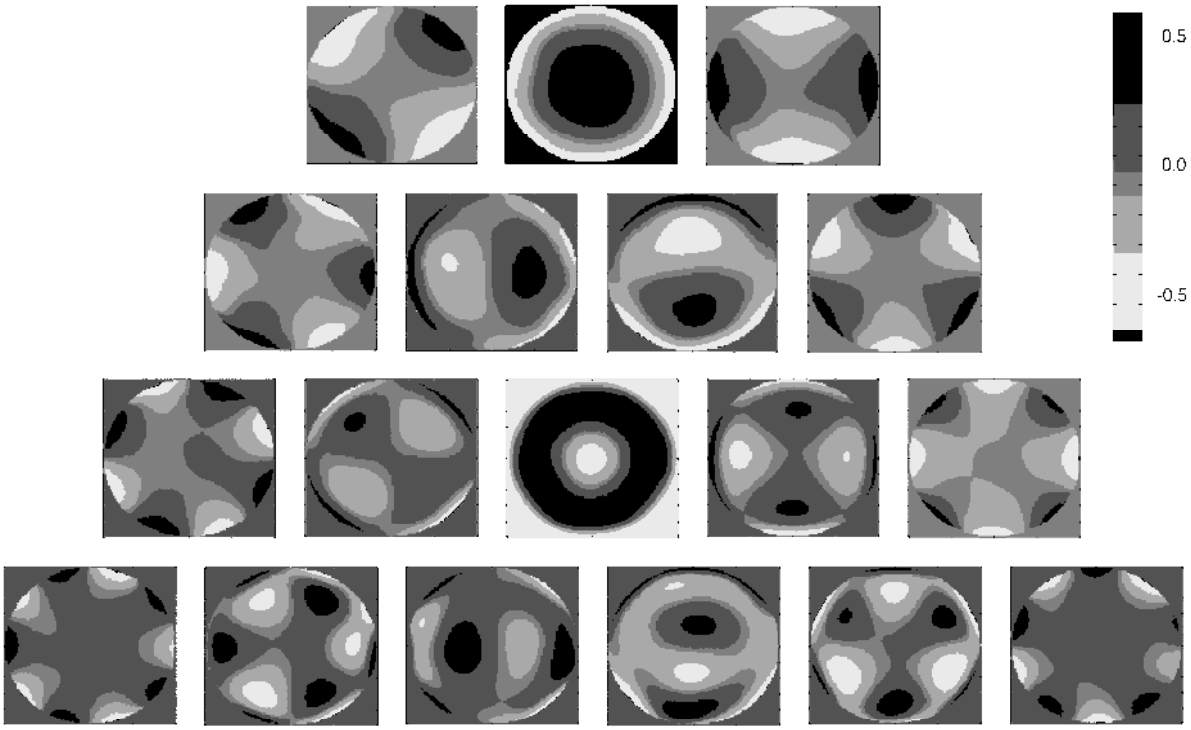

Figure 8: Measured Zernike polynomial shapes produced by the mirror. Scale bars show 1.0μm amplitude in wavefront.

6. Conclusions

An architecture and a manufacturing process for producing robust, high-performance micromachined deformable mirrors has been developed. Through constrained design rules, foundry processing, and special-purpose post processing, mirrors with excellent optical and electromechanical characteristics have been produced. Static and dynamic behavior of individual actuators in the device have been measured, and their characteristic stroke, resolution, repeatability, influence function, and frequency response have proven suitable for wavefront correction in an aberrated optical system. These compact, low-power devices have proven repeatable to nanometer-scale tolerances, and have been used successfully in a number of adaptive optics applications. Such mirrors have immediate uses in microscope and telescope systems for improving image resolution.

The micromachined DM's described in this paper have been used in a number of adaptive optical applications to compensate wavefront aberrations. One promising implementation is in retinal imagaing. The μDM which is closely matched in aperture diameter to the human pupil, has been used to compensate for aberrations in the cornea [5]. As a result, diffraction-limited images of the retina

were obtained for the first time using a MEMS deformable mirror. Conversely this correction can allow vision correction to levels better than 20/20 while simultaneously providing direct measurement to prescribe corrective lenses [7]. Another application is in point-to-point laser communication in which the μDM is used to compensate for atmospheric turbulence and thermal distortions. In this application, the DM described in this paper has been used with considerable success [21].

Future directions for this technology include development of mirrors with thousands of actuators for very-high resolution wavefront control, and development of longer-stroke mirrors for applications requiring compensation of especially large aberrations.

7. Acknowledgments

This work has been supported by grants from the Army Research Office (ARO), the Army Research Laboratory (ARL) and the Defense Advanced Research Projects Agency (DARPA).

8. References

1. J.E. Pearson, S. Hansen, “Experimental studies of a deformable-mirror adaptive optical system,” *J. Opt. Soc. Am*., vol. 67 no. 3, pp. 325-333, 1977.

2. R.J. Tyson, *Introduction to Adaptive Optics*, SPIE Press, Bellingham, Washington, 2000, Chapter 1.

3. T. Weyrauch, M.A. Vorontsov, T. G. Bifano, A. Tuantranont, V. M. Bright, J. R. Karpinsky, J.A. Hammer, “Performance evaluation of micromachined mirror arrays for adaptive optics”, *Proc. SPIE Vol. 4124*, p. 32-41, High-Resolution Wavefront Control: Methods, Devices, and Applications II, November 2000.

4. D. Dayton, j. Gonglewski, S. Restaino, J. Martin, J. Phillips, M. Hartman, S. Browne, P. Kervin, J. Snodgrass, N. Heimann, M. Shilko, R. Pohle, B. Carrion, C.Smith, and D. Thiel, "Demonstration of new technology MEMS and liquid crystal adaptive optics on bright astronomical objects and satellites," Optics Express 10 (25): 1508-1519, 2002.

5. N. Doble, G. Yoon, L. Chen, P. Bierden, B. Singer, S. Olivier, and D. R. Williams, "Use of a microelectromechanical mirror for adaptive optics in the human eye," Optics Letters, Volume 27, Issue 17, 1537-1539, 2002.

6. D. U. Bartsch, , L.J. Zhu, P. C. Sun, S.Fainman, and W. Freeman. "Retinal imaging with a low-cost micromachined membrane deformable mirror," J. Biomed. Opt. [7] (3): 451-456 2002.

7. S.S. Olivier, "Adaptive optics applications in vision science," Proc. SPIE Vol. 5001, p. 50-55, 2003.

8. J. Liang, D.R. Williams and D. Miller, "Supernormal vision and high-resolution retinal imaging through adaptive optics," J. Opt. Soc. Am. A 14, 2884-2892, 1997.

9. S.C. Wilks, C.A. Thompson, S.S. Olivier, B.J. Bauman, L.M. Flath, D.A. Silva, R.M. Sawvel, T.B. Barnes, J.S. Werner, “High-resolution adaptive optics test bed for vision science”, *Proc. SPIE Vol. 4494*, p. 349-356, Adaptive Optics Systems and Technology II, February 2002.

10. M. Vorontsov, G. Carhart, "Adaptive phase distortion correction in strong speckle-modulation conditions," Opt Letters, 27 (24): 2155-2157, 2002

11. T. Weyrauch, M. Vorontsov, "Dynamic wave-front distortion compensation with a 134-control-channel submillisecond adaptive system," Opt Letters, 27 (9): 751-753, 2002

12. T. Weyrauch, M.A. Vorontsov, J. Gowens, T.G. Bifano, “Fiber coupling with adaptive optics for free-space optical communication”, *Proc. SPIE Vol. 4489*, p. 177-184, Free-Space Laser Communication and Laser Imaging, January 2002

13. P.N. Marsh, D. Burns, and J.M. Girkin, " Practical implementation of adaptive optics in multiphoton microscopy," Optics Express 11 (10): 1123-1130, 2003

14. M.R. Armstrong, P. Plachta, E.A. Ponomarev, R.J.D. Miller, " Versatile 7-fs optical parametric pulse generation and compression by use of adaptive optics," Optics Letters 26 (15): 1152-1154, 2001.

15. E. Calloni, J.T. Baker, F. Barone, "Adaptive optics approach for prefiltering of geometrical fluctuations of the input laser beam of an interferometric gravitational waves detector," Rev Sci. Instrum 74 (4): 2570-2574, 2003

16. J.A. Perreault, P.A. Bierden, M.N. Horenstein, T.G. Bifano. “Manufacturing of an optical quality mirror system for Adaptive Optics”. Proceedings of SPIE Vol. 4493, p. 13-20, 2001.

17. R. K. Mali, T.G. Bifano, D. A. Koester, “Design-based approach to planarization in multilayer surface micromachining,” J. Micromech. Microeng., pp. 294–299, 1999.

18. T. Bifano, H. Johnson, P. Bierden, R. Mali, "Elimination of Stress-Induced Curvature in Thin-Film Structures", Journal of Microelectromechanical Systems, Vol 11, No. 5, p. 592-597, October 2002

19. P. Krulevitch, P. Bierden, T. Bifano, E. Carr, C. Dimas, H. Dyson, M. Helmbrecht, P. Kurczynski, R. Muller, S. Olivier, Y. Peter, B. Sadoulet, O. Solgaard, and E.H. Yang,"MOEMS spatial light modulator development at the Center for Adaptive Optics," *Proceedings of SPIE Vol. 4983*, 2003

20. T. F. Miyahira , H. D. Becker, S. S. McClure, L. D. Edmonds, A. H. Johnston, "Total Dose Degradation of Optical MEMS Mirrors," 2003 IEEE Nuclear & Space Radiation Effects Conference, Monterrey, CA, 21 - 25 Jul 2003

21. 21. Weyrauch, T., Vorontsov, M. A., Gowens, J., and Bifano, T. G., "Fiber coupling with adaptive optics for free-space optical communication," *Proc. SPIE Vol. 4489,* p. 177-184, Free-Space Laser Communication and Laser Imaging; David G. Voelz, Jennifer C. Ricklin; Eds., Jan 2002